Supporting Information for

Characterization of Microplastics in Clouds over Eastern China

Xinmiao Xu[a,#], Tao Li[a,b,#], Jiebo Zhen[a], Yuqian Jiang[a], Xiaoling Nie[a], Yan Wang[a*], Xian-Zheng Yuan[a], Xinfeng Wang[c], Likun Xue[c], Jianmin Chen[d]

[a] School of Environmental Science and Engineering, Shandong University, Qingdao 266237, China

[b] Division of Environment and Sustainability, The Hong Kong University of Science and Technology, Kowloon, Hong Kong 999077, China

[c] Environment Research Institute, Shandong University, Qingdao 266237, China

[d] Department of Environmental Science and Engineering, Fudan University, Shanghai 200433, China

Corresponding author: Y. Wang (wy@sdu.edu.cn)

[#] Xinmiao Xu and Tao Li contributed equally to this work.

This file contains:

7 texts

13 figures

6 tables

Text S1. Site description

The summit of Mt. Tai (36.25°N, 117.10°E, 1545 m a.s.l., Fig. S1) is the highest point in Shandong province, eastern China, serving as an atmospheric regional background station in the North China Plain.[1] It is situated 15 km north of Tai'an city (with a population of 5.47 million) and 30 km south of Jinan city (the capital city of Shandong province with a population of 9.20 million). To the east are Bohai Sea and Yellow Sea with the nearest distance of about 230 km. Due to diurnal variation of the boundary layer height, the summit is usually immersed within atmospheric boundary layer during the daytime and above it at night, influenced by air pollution resulting from both local emission and long-range transport. Dominated by the East Asian Monsoon, Mt. Tai frequently experiences clouds and precipitation in summer (June to October), making it an ideal platform to collect cloud water samples.[2]

Text S2. Cloud event definition and chemical analysis of samples

(a) Definition a cloud event and a sample

The start and end time of cloud events and samples listed in Table S1 were recorded mainly based on the on-site visual identification. The concrete indices, i.e. cloud droplet number concentration (Nd, #/cm^3) and liquid water content (LWC, g m^3) monitored by a fog monitor (FM-120, Droplet Measurement Technologies Inc., USA), and the relative humidity (RH) measured by the Taishan National Reference Climatological Station, were used to assist in defining a cloud event.

In empirical, the start time of a cloud event is recorded when LWC is higher than ~0.01 g m^{-3}, Nd exceeds ~50 cm^{-3}, and accordingly RH is over 98%. It is regarded as the end of a cloud event if there are no visual clouds on the mountaintop upon dissipation, or Nd of the remnants of the clouds is less than 50 cm^{-3} and LWC is lower than 0.01 g m^{-3}, below which the cloud water is hardly collected, for 1–2 hours. Usually only one cloud water sample was collected during a short-time cloud event (several hours) to ensure the sample volume for chemical analysis. However, several samples could be collected during a long-time continuous cloud

event (one to two days). For example, there were 5 samples (ID 9–13) were collected during the cloud event IX (Table S1). Approximately 3–6 hours are needed for collecting one sample with enough volume.

(b) Chemical analysis

In-situ measurements of pH, electrical conductivity (EC) and water temperature were conducted immediately after cloud water collection using a portable pH meter (Model 6350M, JENCO). Ion chromatography (Metrohm 940, Switzerland) was used to measure concentrations of water-soluble inorganic ions (F^-, Cl^-, Br^-, NO_3^-, SO_4^{2-}, NH_4^+, Na^+, K^+, Ca^{2+} and Mg^{2+}). Dissolved organic matter (DOM) were quantified using a TOC analyzer (TOC-L CPH/CPN, SHIMADZU, Japan) through NDIR detection of CO_2 after thermocatalytic oxidation at 650 °C. Dissolved Hg was determined by a cold vapor atomic fluorescence spectrometry (CVAFS, Brooks Rand MERX 24400, USA) following the US EPA method 1631 E. Dissolved trace elements, including Li, Be, B, Al, Ti, V, Cr, Mn, Fe, Co, Ni, Cu, Zn, As, Se, Sr, Mo, Ag, Cd, Sn, Sb, Ba, Pb and Bi, were analyzed using Inductively Coupled Plasma Mass Spectrometry (Thermo scientific iCAP RQ ICP-MS, USA).

Text S3. MPs extraction and blank control

To minimize the interference of organic substances, the filtered cloud water residues on PTFE membrane (47 mm diameter, 0.22 μm pore size, ANPEL Laboratory Technologies (Shanghai) Inc) were digested by 15 mL of 30% v/v H_2O_2 at 60 °C for 5 h. After digestion, the sample was filtered through a new PTFE membrane, rinsed with 250 mL Milli-Q ultrapure water. The filtered material was flushed into a density separation funnel with saturated $ZnCl_2$ solution to separate microplastics (MPs) from other impurities with higher density. After settling for 48 h, the settled material was drained away, while the remaining sample in the upper layer were filtered, and the funnel was rinsed onto the filter with 200 mL Milli-Q ultrapure water. The filter was then dried and transferred to a sealed box for MPs examination. We observed that the cloud water residues had very few impurities, and thus the density separation process was omitted to reduce losses.[3]

A total of 9 blank samples were obtained, including field blanks, laboratory blanks and membrane blanks. The Teflon strings of the cloud water collector were rinsed gently by spraying 500 mL of Milli-Q ultrapure water, and three water samples were collected as field blanks (FB). Three laboratory blanks (LB) were obtained through digestion, density separation, and filtration of 500 mL of Milli-Q ultrapure water. Three membrane blanks (MB) were also examined to check any potential contamination of the membrane used for MPs filtration. The results of the blank samples are presented in Table S2.

All labware used in the experiments were glass or stainless steel and was rinsed with Milli-Q ultrapure water before use. The experiments were conducted in well-ventilated settings. Cotton lab coats and nitrile gloves were worn to minimize the possibility of contamination from synthetic textiles.

Text S4. Instrumental Analysis

Stereo microscope

The pretreated debris retained on the PTFE membrane was inspected and photographed under a stereo microscope (Olympus SZX7, Tokyo, Japan). Fibers and particles that suspiciously appeared to be plastic were identified through visual analysis of their shape, color, morphology, and physical characteristics. In this study, we categorized microplastics into four groups based on their shape: (a) fibers, which are plastic filaments or elongated particles with a uniform width and an aspect ratio greater than 3:1, (b) fragments, which have irregular shapes with sharp edges and cracked surfaces, (c) films, which are irregularly thin and soft particles with a flat plane and less sharp edges, and (d) spheres, which are spherical or ellipsoidal microbeads.

The polymer types of these suspected microplastics were further tested and identified using a micro-Fourier transform infrared spectroscopy (FTIR) for MPs with a size larger than 50 μm given the minimum limit size of 10 μm.[4] A Raman spectroscopy with a lower minimum limit size of 1 μm was used for further identifying MPs smaller than 50 μm.

To our knowledge, smaller plastic particles such as nanoplastics (NPs) have the potential to aggregate to larger particles but with an upper limit size of ~5 μm. However, the cloud MPs identified based on our methods were larger than 8 μm, among which no NP aggregates were observed. Thus, we believe that the MPs concentrations in this study were not overestimated due to the possible NPs aggregation during filtration.

FTIR

The micro-Fourier transform infrared system (Thermo scientific Nicolet iS5, USA) was used to identify the types of MP particle polymers. The scanning spectral range was set to 4000–650 cm^{-1} with a resolution of 8 cm^{-1}. The detector ran 32 scans for each particle and cooled using liquid nitrogen. The spectrum was calibrated by retesting background for each particle sample.[5] Spectral matching between particles and standard materials was done using OMNIC software (Thermo Electron Corporation, 17 Waltham, MA, USA). The reference databases included OMNIC spectra library and Hummel Polymer and Additives FT-IR Spectral Library. Similarities above 70% were considered indicative of the exact polymer.[4]

Raman Spectroscopy

A Raman Microscope (Thermo scientific DXR2, USA, spectral range of 50–3200 cm^{-1} with a resolution of 1.5 cm^{-1} and confocal imaging accuracy of 0.5 μm) was used to analyze the total plastic presence with a 785nm laser (spatial resolution of 1 μm) and a 200–2000 cm^{-1} Raman shift range under 10X objective. The spectra were collected using an acquisition time of 15 s and ten accumulations at 8mW laser energy (50 μm slit, grating 400 lines/mm), and each sample was tested twice for accuracy. The spectra were compared with spectroscopy Edition and Open spectra source databases using KnowItAll Informatics System 2021 to provide a clear definition of the chemical and bond spectra peaks.

SEM-EDX

The surface micromorphology and elemental composition of the identified MPs were studied using the Scanning Electron Microscope (Gemini SEM 300, Carl Zeiss, Germany) with

Energy-dispersive X-ray spectroscopy (SEM-EDX) under 20 KV voltage. The selected MP particles were placed on the stub using double-sided tape, and then sprayed with Platinum coating to make them conductive. EDX elemental mapping image was obtained for visualizing the distribution of trace elements on the surface of MP particles.

Text S5. Data Processing

Given the large number of MPs and analysis constraints, it is not possible to count all MP particles in a complete filter. We follow the scaling approach by Allen et al. (2019) which analyzed MPs in atmospheric deposition,[6] assuming that the filtered MPs are evenly retained on the membrane as the cloud water samples have been well shaken before quick filtration. A quarter of the filters was visually inspected to satisfactorily count and confirm the large MPs (size >50 μm) with FTIR. Three 4×4 mm^2 areas of the filters were randomly selected for counting small MPs (size <50 μm) confirmed with Raman. The MP count for the sample area of Raman analysis was averaged as:

$$\bar{X}_{Raman} = \frac{\sum_{i=1}^{n} X_i}{n} \quad (1)$$

where $\bar{X}_{Raman}$ is the average count of MPs (with size smaller than 50 μm) for a sample area identified by Raman spectroscopy, X_i is the MPs count for the *i*th sample area, n is the number of sample area examined by Raman.

The concentration of MPs per filter was calculated through a sum of MP counts per sample area, scaling using known filter area and cloud water volume (L) or airmass volume (m^3), following the equations below:

$$X_{total} = \frac{X_{FTIR} \times S}{S_{FTIR}} + \frac{\bar{X}_{Raman} \times S}{S_{Raman}} - X_{Blank} \quad (2)$$

where X_{total} is the total count of MPs per filter, S is the total effective area of the filter membrane, S_{FTIR} is the sample area of FTIR detection (a quartile of the filter), S_{Raman} is the sample area in Raman detection (1.6×10^{-5} mm^2), X_{Blank} is the average number of MPs found on the blank samples.

To compare with the MPs concentrations reported in other atmospheric fallout,[7] in this study we quantified the MPs concentration in clouds with the unit of both MP L^{-1} and MP m^{-3}:

$$C_{liquid\ phase} = \frac{X_{total}}{V_{cloud\ water}/1000} \quad (3)$$

$$C_{gas\ phase} = \frac{X_{total}}{V_{airmass\ of\ clouds}} \quad (4)$$

$$V_{airmass\ of\ clouds} = \frac{V_{cloud\ water}}{LWC/\rho} \quad (5)$$

where $C_{liquid\ phase}$ is the concentration of MPs in liquid cloud water, MP L^{-1}, $V_{cloud\ water}$ is the volume of collected cloud water sample (mL), $C_{gas\ phase}$ is the concentration of MPs in the airmass of clouds, MP m^{-3}, $V_{airmass}$ is the volume of clouds in the air (m^3), *LWC* is the cloud liquid water content (g m^{-3}), ρ is the density of cloud water (1.0 g/mL). Note that cellulose identified in this study was not counted as microplastics because of their uncertain natural or anthropogenic/synthetic origin.

Text S6. MPs aging and adsorption simulations

Photo(chemical) aging is an important and inevitable weathering process for MPs suspended in the atmosphere.[8] Hence we tried to evaluate the adsorption behavior of photoaged MPs in cloud water. To this end, laboratory simulations of MPs photoaging and adsorption were performed with five types of model MPs (150 mesh, <100 μm, Guangdong Hengfa Plasticizing Co., LTD.), i.e., polyamide (PA), polypropylene (PP), polystyrene (PS), polyethylene (PE, 20%), and polyethylene terephthalate (PET). Following the methods described in previous studies,[9, 10] three sets of 0.05 g model MPs were prepared in quartz tubes and subjected to photoaging in ambient air, ultrapure water (20 ml), and a real nighttime cloud water sample (20 ml, with chemical composition shown in Table S3) under UV light irradiation (100 W mercury lamp, 254 nm) for 96 hours with regular stirring, respectively.

These photoaged MPs were subsequently added into aliquots (20 ml each) of the real cloud water sample (Table S3) separately and shaken in the dark to simulate adsorption process. After 12 hours of adsorption, 5 ml of the MPs solution was collected, filtered, and dried, and

then inspected under a stereo microscope. The surface elemental composition of both pristine and photoaged MPs was semi-quantified and mapped using SEM-EDX analysis.

Text S7. HYSPLIT and CWT models

To identify the contribution of air masses transport to MPs in clouds, the NOAA Hybrid Single Particle Lagrangian Integrated Trajectory (HYSPLIT) model (PC version 4.8) was used to reconstruct three-day backward trajectories of air masses for clouds arriving at Mt. Tai at the height of 1545 m a.s.l. Trajectories were initiated every hour and calculated during the observation period. The archived GDAS meteorological data with a horizontal resolution of 1° latitude-longitude was used to drive the model.

Based on the HYSPLIT trajectories and measured MPs concentration, the concentration-weighted trajectory (CWT) model was employed to identify the potential source regions of MPs. CWT can calculate the weighted abundance of the trajectory and reflect its pollution degree. The calculation method is as follows:

$$CWT_{ij} = \sum_{i=1}^{N_l} C_l \tau_{ijl} \Big/ \sum_{i=1}^{N_l} \tau_{ijl} \quad (6)$$

where CWT_{ij} represents the average weighted concentration in the ij_{th} cell, C_l is the MPs concentration corresponding to the trajectory l, N_l is the total number of trajectories, τ_{ijl} is the number of trajectory segment endpoints in ij_{th} grid cell for the trajectory l, i.e., residence time of the trajectory l in the ij_{th} cell.

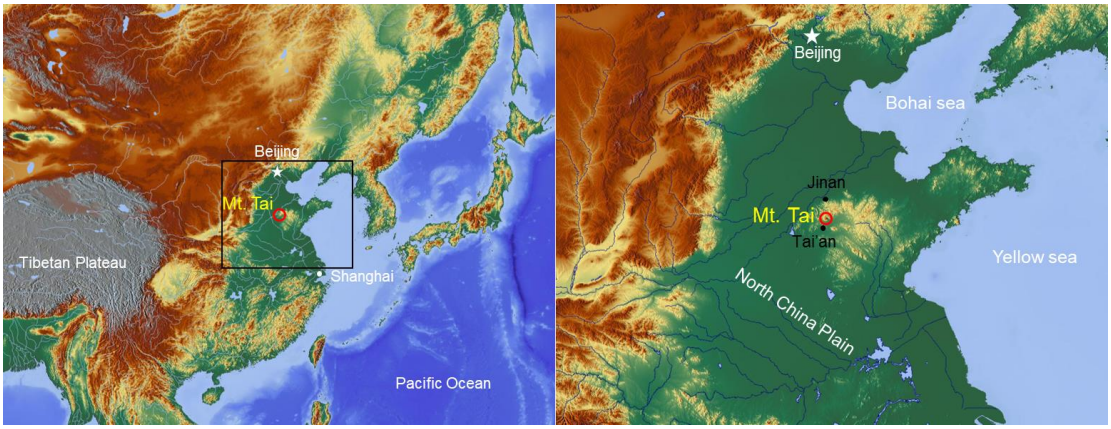

Figure S1. Geographic location of the sampling site at Mt. Tai (red triangle).

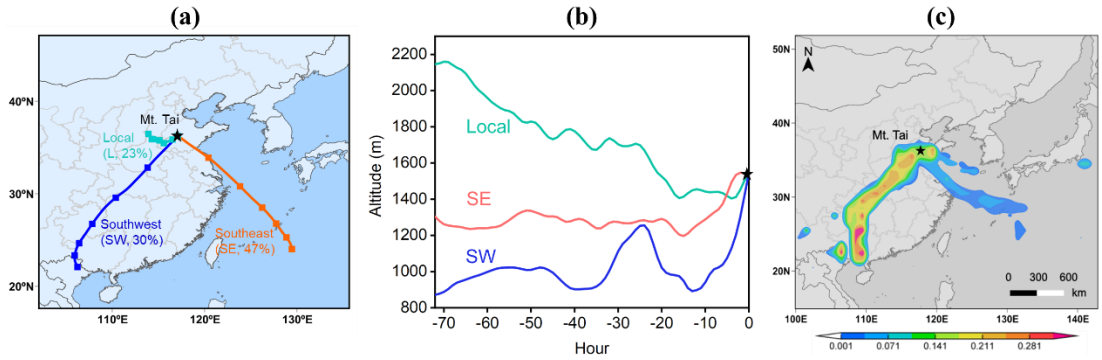

Figure S2. (a) Clusters of 72-hour backward trajectories arriving at Mt. Tai during the observation period, (b) the average height of each cluster trajectory, and (c) CWT result of MPs concentration.

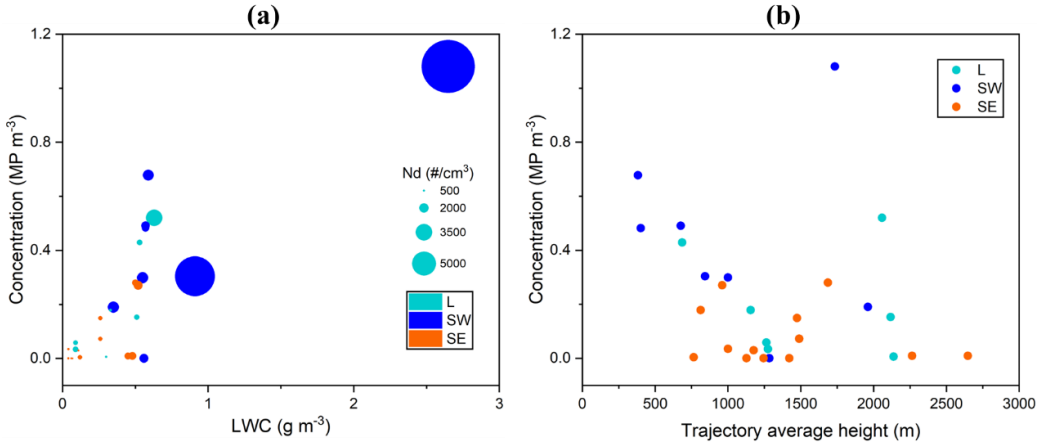

Figure S3. MPs concentrations *versus* (a) LWC, and (b) average height of backward trajectories. The cloud droplet number concentration (Nd) is indicated by the size of cycles. The local (L), southwest (SW), and southeast (SE) clusters are denoted by colors.

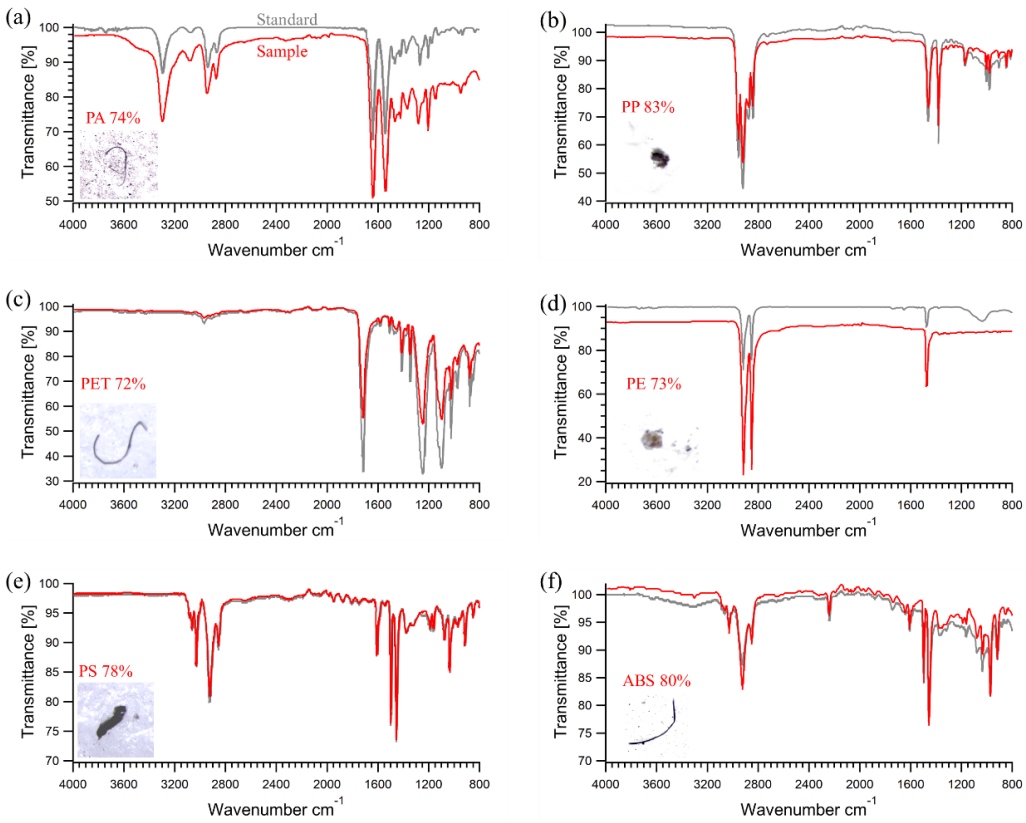

Figure S4. FTIR spectra of polymers identified from cloud water samples. Gray lines show spectra of standard polymers for reference. Red lines indicate spectra of samples. The percentage number refers to the degree of spectral matching between samples and standard polymers. The spectra are for polymers (a) polyamide (PA), (b) polypropylene (PP), (c) polyethylene terephthalate (PET), (d) polyethylene (PE), (e) polystyrene (PS), and (f) acrylonitrile butadiene styrene (ABS).

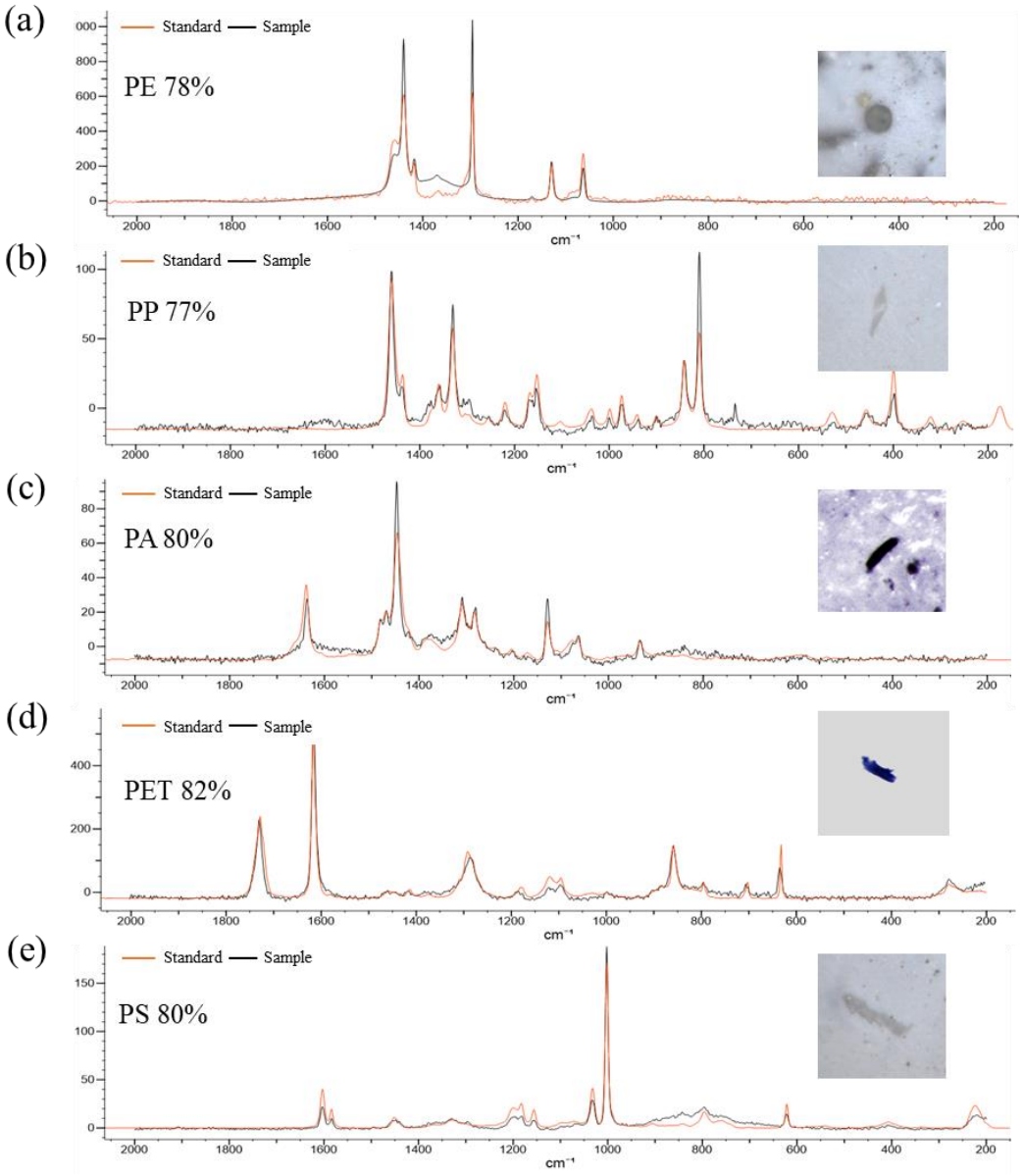

Figure S5. Raman spectra of polymers identified from cloud water samples. Orange lines show spectra of standard polymers for reference. Black lines indicate spectra of samples. The percentage number refers to the degree of spectral matching between samples and standard polymers. The spectra are from polymers (a) polyethylene (PE), (b) polypropylene (PP), (c) polyamide (PA), (d) polyethylene terephthalate (PET), and (e) polystyrene (PS).

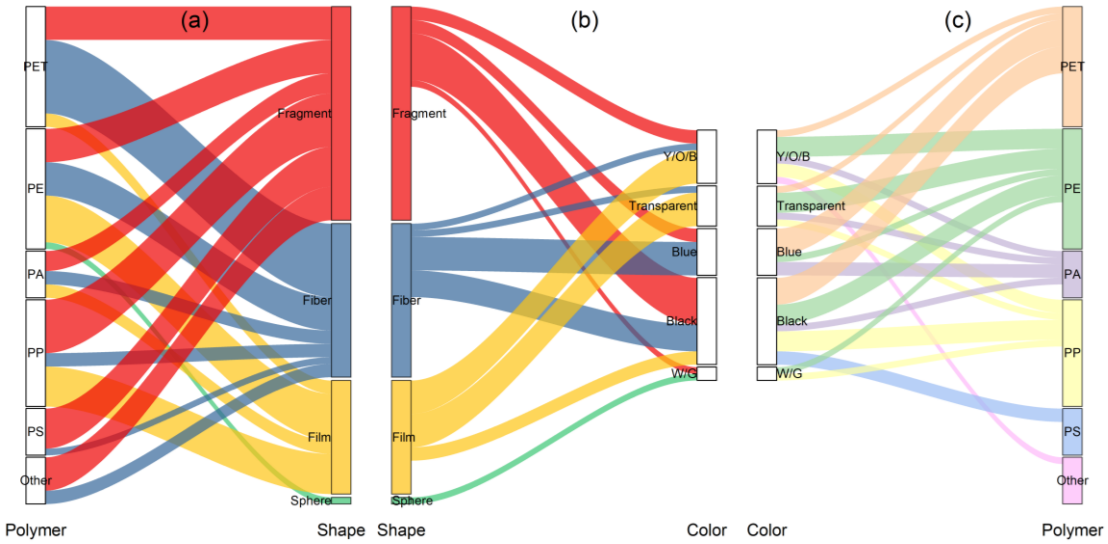

Figure S6. Alluvial diagrams illustrating the associations between (a) polymer and shape, (b) shape and color, and (c) polymer and color. Y/O/B: yellow/orange/brown; W/G: white/gray. Note that the color of MPs smaller than 50 μm cannot be accurately recognized under the microscope, so only the MPs larger than 50 μm were included in the color category.

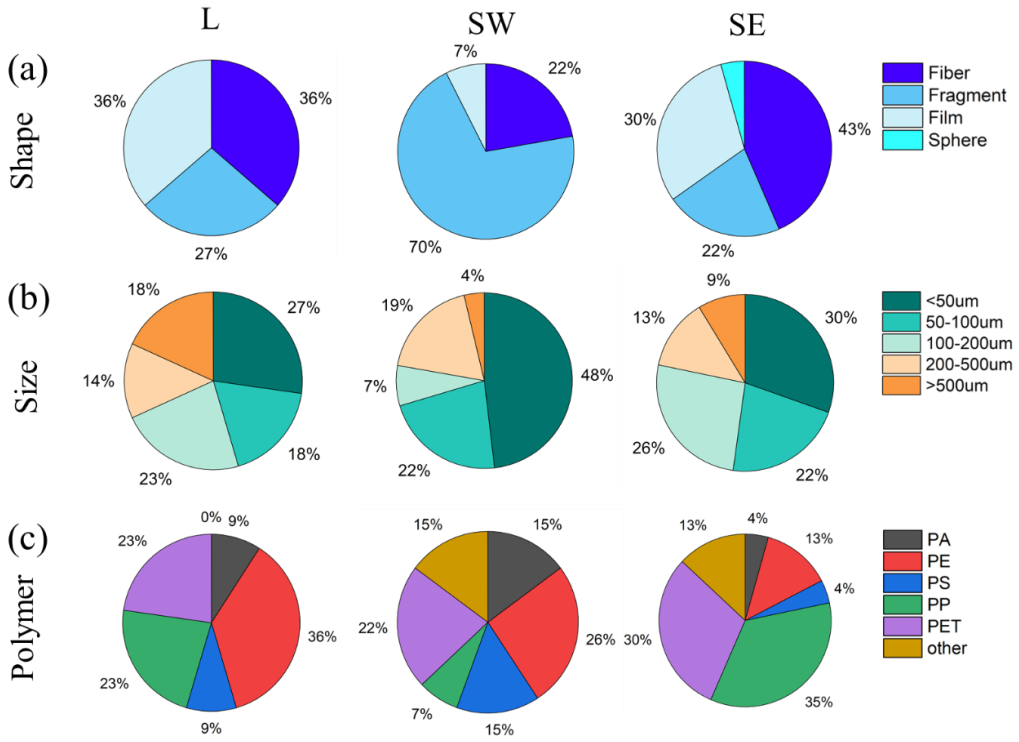

Figure S7. MP compositions in clouds in terms of (a) shape, (b) size, and (c) polymer from different clusters (L, SW, and SE).

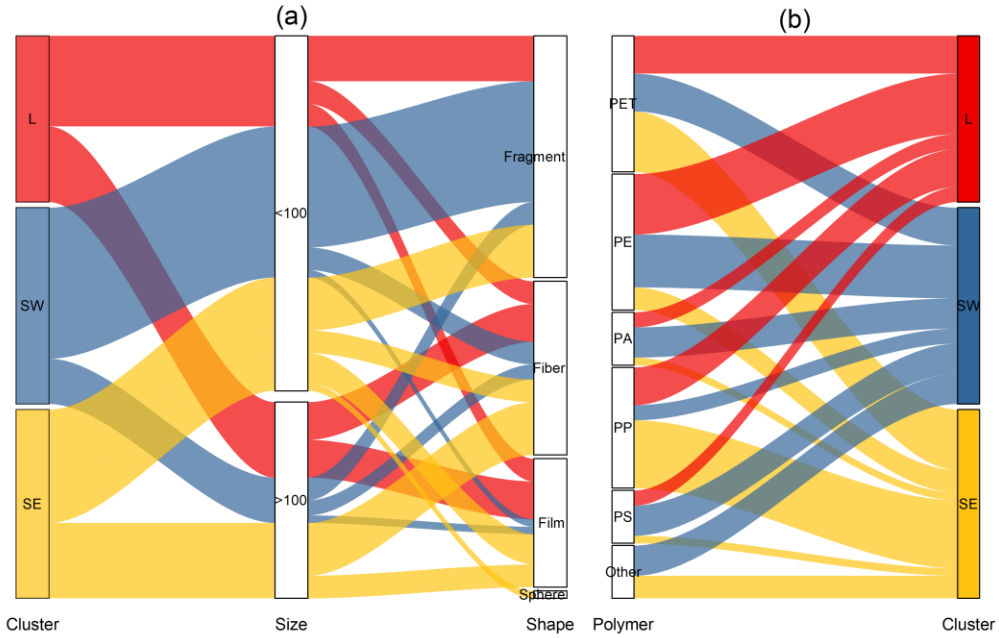

Figure S8. Associations of cluster (L, SW, and SE) with the (a) size and shape, and (b) polymer of MPs. The sizes are simply divided into two categories, smaller and larger than 100 μm, which is a size for defining total suspended particulate matter.

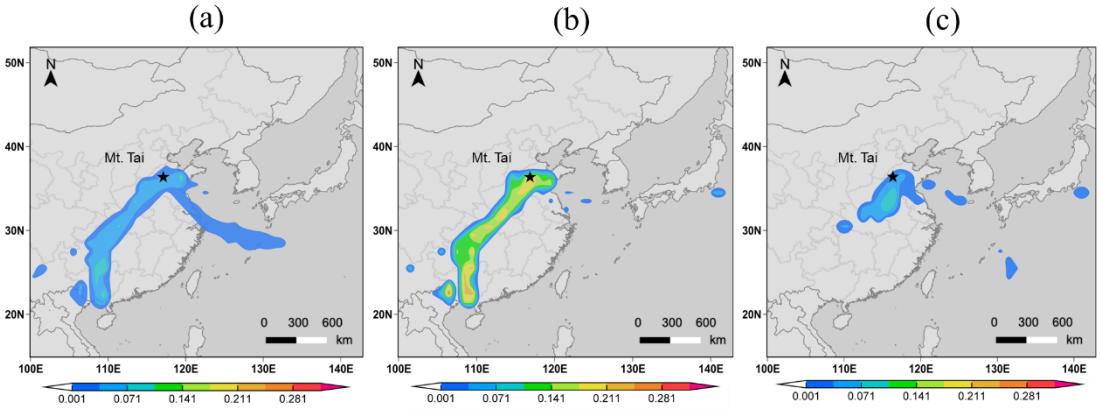

Figure S9. Potential source regions of MPs in clouds at Mt. Tai during the observation period in the forms of (a) fiber, (b) fragment, and (c) film as identified by CWT analysis. Color scale represents the probability of MPs presence (MP m^{-3}).

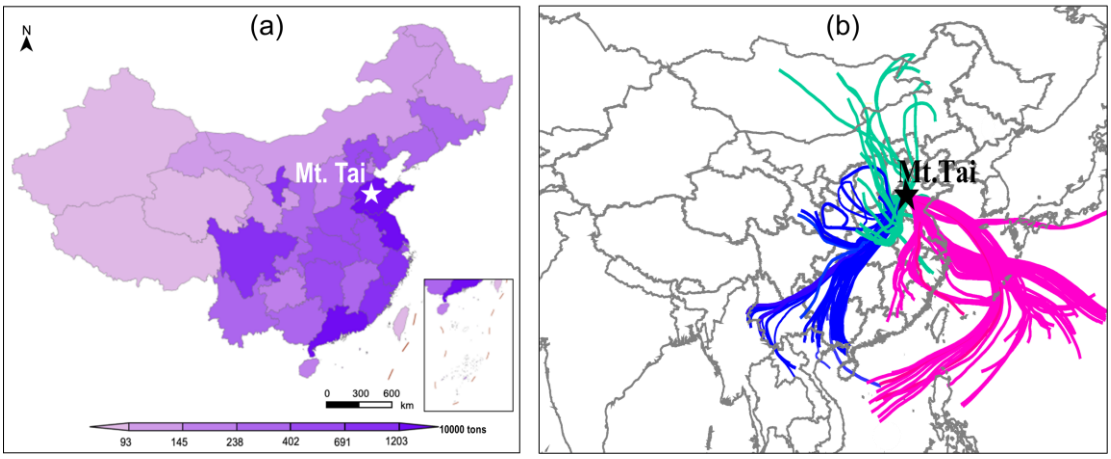

Figure S10. (a) The capacity of municipal solid waste incineration by province (10000 tons) as represented by color scale, and (b) three-day backward trajectories colored for clusters. Data are from the National Bureau of Statistics of China, 2020.

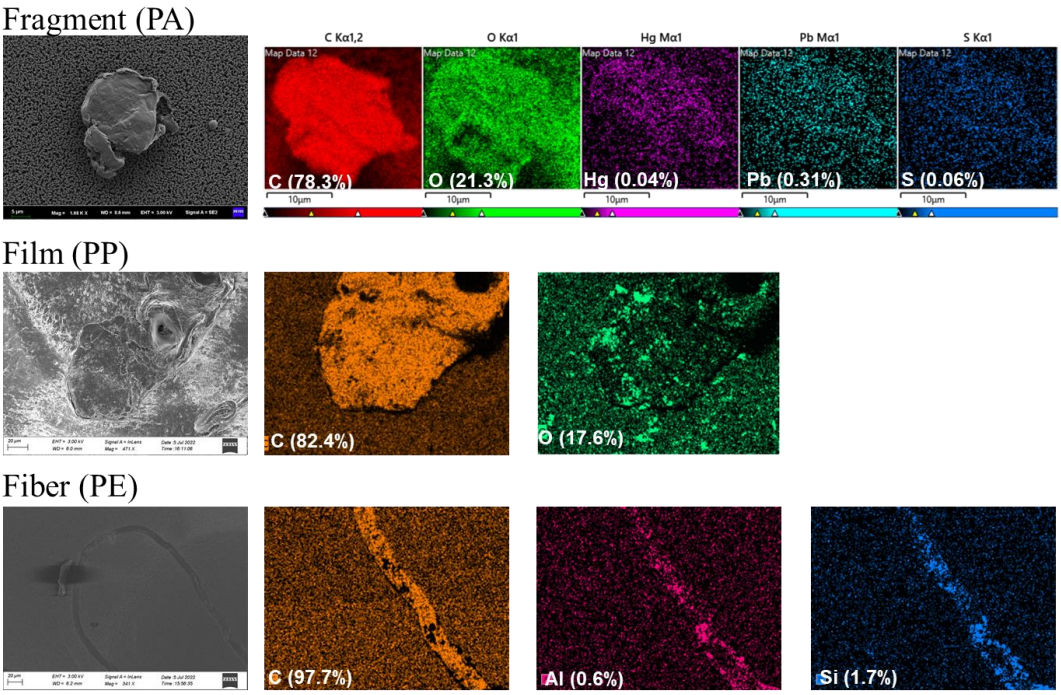

Figure S11. SEM images and element mapping of microplastic fragment, film and fiber in clouds at Mt. Tai. The mass fraction (in brackets) of detected elements was semi-quantified by EDX analysis. Note that only elements exceeding 0.01% of total mass can be determined. Al and Si on the fiber indicate the adhesion of mineral nanoparticles.

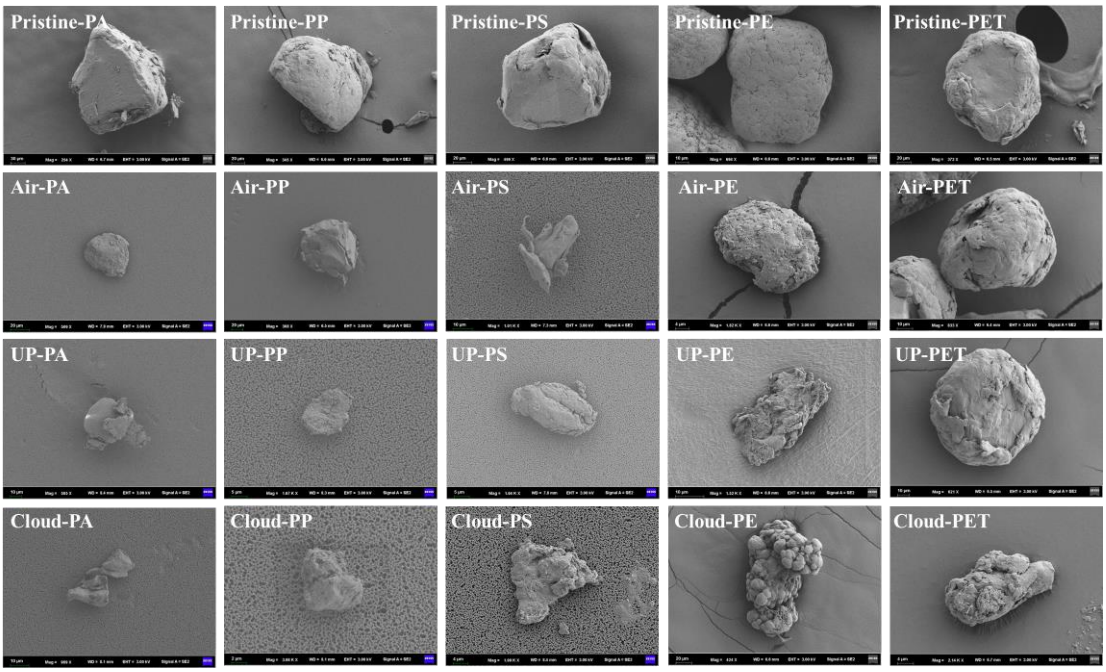

Figure S12. SEM images of pristine and photoaged MP model particles (PA, PP, PS, PE and PET) in ambient air (Air), ultrapure water (UP), and a nighttime cloud water sample (Cloud).

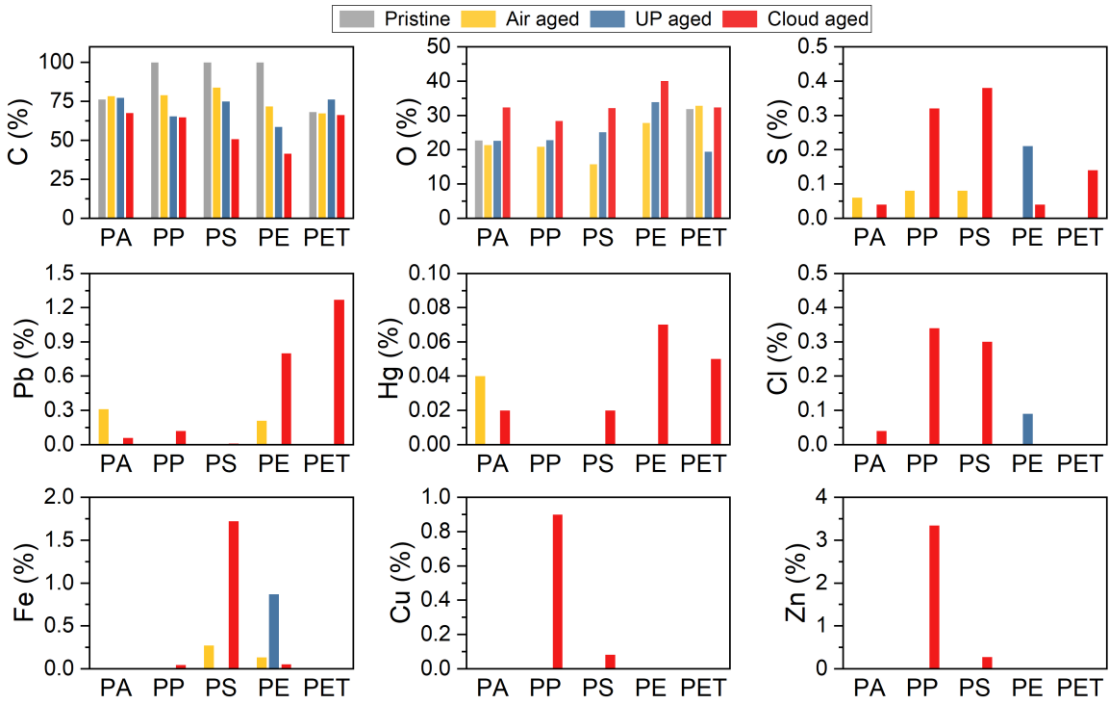

Figure S13. Elemental composition (%) semi-quantified using SEM-EDX analysis on the surface of pristine and photoaged MP particles in air, UP water, and cloud water (denoted by color bars) after adsorption simulation.

Table S1. Sampling information of cloud water at Mt. Tai in summer 2021 and identified microplastics with classification into different categories. (see the Supporting Information EXCEL file)

Table S2. Examination of MPs in the blank samples.

Blanks	Blank ID	MPs count (item per sample)	Mean
Field blank 1	FB-1	3	
Field blank 2	FB-2	1	2
Field blank 3	FB-3	2	
Laboratory blank 1	LB-1	2	
Laboratory blank 2	LB-2	0	1
Laboratory blank 3	LB-3	1	
Membrane blank 1	MB-1	0	
Membrane blank 2	MB-2	0	0
Membrane blank 3	MB-3	0	

Table S3. Chemical composition of the nighttime cloud water sample used for MPs photoaging and adsorption experiments.

Component	Unit	Concentration	Component	Unit	Concentration
DOC	mg L^{-1}	25.01	Mn	ng L^{-1}	113.4
NH_4^+	mg L^{-1}	29.4	Fe	ng L^{-1}	198.1
K^+	mg L^{-1}	0.98	Co	ng L^{-1}	1.36
Ca^{2+}	mg L^{-1}	10.61	Ni	ng L^{-1}	44.9
Mg^{2+}	mg L^{-1}	0.49	Cu	ng L^{-1}	11.57
F^-	mg L^{-1}	0.71	Zn	ng L^{-1}	599.4
Cl^-	mg L^{-1}	2.83	As	ng L^{-1}	8.99
Br^-	mg L^{-1}	0.62	Se	ng L^{-1}	32.39
NO_3^-	mg L^{-1}	72.8	Sr	ng L^{-1}	30.54
SO_4^{2-}	mg L^{-1}	41.3	Mo	ng L^{-1}	1.41
Hg	ng L^{-1}	99.8	Ag	ng L^{-1}	0.24
Li	ng L^{-1}	1.61	Cd	ng L^{-1}	1.44
Be	ng L^{-1}	0.03	Sn	ng L^{-1}	1.35
B	ng L^{-1}	48.5	Sb	ng L^{-1}	2.06
Al	ng L^{-1}	134.2	Ba	ng L^{-1}	34.67
Ti	ng L^{-1}	63.4	Pb	ng L^{-1}	3.22
V	ng L^{-1}	24.5	Bi	ng L^{-1}	0.22
Cr	ng L^{-1}	4.53			

Note: This cloud water sample was collected at night from 23:00 on June 28 to 5:30 on June 29.

Table S4. Concentrations of airborne MPs in clouds at Mt. Tai in this study and in fallout reported in literatures.

Location	Sample	Environment	MPs conc. (m^{-3} or L^{-1})	Mean or median	Size range (μm)	Predominant size (μm)	Analytical method
Mt. Tai (this study)	Cloud water	Rural mountain	0−1.08[a] *0−1154*[b]	0.21[a] *462.5*[b]	8−1542	<100	FTIR + Raman
Mt. Tai[11]	Rainfall	Rural mountain	*0−858*[b]	*178*[b]	20−1993	<250	FTIR + Raman
Aquitaine, France[12]	Sea mist	Coast	0.02−0.19[a]	0.06[a]	8−140	24±14	Raman
Mt. Oyama and Mt. Fuji, Japan[13]	Cloud water	Rural mountain		*6.7−13.9*	7.1−94.6	29.9−38.3	FTIR
Mt. Derak, Iran[14]	Rainfall	Mountain	*0−680*[b]	*145*[b]		<100	Raman
Nam Co Basin, Tibetan Plateau, China[4]	Rainfall	Remote terrestrial	*9.8−37.5*[b]	*21.9*[b]			FTIR
Nam Co Basin, Tibetan Plateau, China[4]	Glacier runoff	Remote terrestrial	*0.175−0.675*[b]	*0.5*[b]	50−3000	300−1000	FTIR
Demula Glacier, Tibetan Plateau, China[15]	Snowpit	Remote terrestrial	*0−36.09*[b]	*9.55*[b]	48−1000	<200	Raman
Arctic snow[5]	Snow	Polar	*0−14.4×10*^{3} [b]	*180* [b]	11−475	<25	FTIR
Antarctic snow[16]	Snow	Polar	*4−82*[b]	*29.4*[b]	50−3510	<1000	FTIR
Shanghai, China[17]	TSP	Urban	0−4.18[a]	1.42[a]	23−5000	<1000	FTIR
Pairs, France[18]	TSP	Urban	0.3−1.5[a]	0.9[a]	50−5000	20−250	FTIR
Pic du Midi, France[7]	PM_{10}	Remote mountain	0.09−0.66[a]	0.23[a]	3−53	<20	Raman
Northwestern South Chin Sea[19]	TSP	Marine	0.013−0.063[a]	0.035[a]	50−2210	<1000	FTIR
West Pacific Ocean[20]	TSP	Coast to open ocean	0−1.37[a]	0.01[a]			FTIR
Pearl River Estury to Indian Ocean[21]	TSP	Open ocean	0−0.077[a]	0.01[a]	58−2252	851	FTIR

Table S5. Proportions of MP colors from different samples in different environments.

Environment	Study area	Sample	Black	Blue	Transparent	White/Gray	Coloful*	Ref
Atmosphere	East Indian Ocean	TSP						[1]
	South China Sea	TSP						[1]
	Mt. Tai, north China	**Clouds**						this study
	Pearl River Estuary	TSP						[1]
	Shanghai, east China	TSP (average)						[2]
	South China Sea	TSP						[3]
	Incineration plant	Fly ash fiber						[4]
Deposition	Wuhan, central China	Urban rainwater runoff						[5]
	Mt. Tai, north China	Rainfall						[6]
	Yantai, north China	Atmospheric deposition						[7]
	Lanzhou, northwest China	Atmospheric deposition						[8]
	Beijing, north China	Rainfall						[9]
	Guangzhou, south China	Atmospheric deposition						[10]
High mountain	DML, southeast Tibetan Plateau	Snowpit						[11]
	Central Italian Alps	Forni Glacier						[12]
	Antisana Glacier, northern Ecuador	Surface snow						[11]
	Nam Co, central Tibetan Plateau	Atmospheric deposition						[13]
Ocean	Global	Seawater						[14]
	Global	Ocean surface water						[15]
	Xisha Islands, South China Sea	Ocean surface water						[16]
Fresh water	China and abroad	Water bodies						[17]
	Headstream of the Yangtze River	Surface water						[18]
	Donghu, Wuhan, central China	Surface water						[19]
Soil in China	Suburbs of Shanghai	Shallow soil						[20]
		Deep soil						[20]
	Sichuan, southwest China	Cultivated Soil						[21]
	Sichuan, southwest China	Non-mulched soil						[22]
		4-year mulched paddy soil						[22]
		10-year mulched paddy soil						[22]
	Five regions across China	Farmland soil						[23]
	Hebei, north China	Mulching cultivated soil						[24]
	Shouguang in Northern China	Agricultural soil						[25]
	Qinghai-Tibet plateau	Shallow soil						[26]
		Deep soil						[26]
	Coastal plain in east China	Soil						[27]
	Sheshui River, central China	Paddy suface soil						[28]
	Mainland China	National farmland soil						[29]

TSP is the total suspended particulate.

* The colorful category includes yellow, orange, brown, red, green and beige.

References [1–29]:

[1] Wang, X., Li, C., Liu, K., et al. Atmospheric microplastic over the South China Sea and East Indian Ocean: abundance, distribution and source. J. Hazard. Mater. 2020; 389: 121846.

[2] Liu, K., Wang, X., Fang, T., et al. Source and potential risk assessment of suspended atmospheric microplastics in Shanghai. Sci. Total. Environ. 2019; 675: 462-471.

[3] Ding, Y., Zou, X., Wang, C., et al. The abundance and characteristics of atmospheric microplastic deposition in the northwestern South China Sea in the fall. Atmos. Environ. 2021; 253: 118389.

[4] Shen, M., Hu, T., Huang, W., et al. Can incineration completely eliminate plastic wastes? An investigation of microplastics and heavy metals in the bottom ash and fly ash from an incineration plant. Sci. Total. Environ. 2021; 779: 146528.

[5] Sang, W., Chen, Z., Mei, L., et al. The abundance and characteristics of microplastics in rainwater pipelines in Wuhan, China. Sci. Total. Environ. 2021; 755: 142606.

[6] Xu, X., Zhen, J., Jiang, Y., et al. Characteristics and sources analysis of microplastics in precipitation of Mount Tai. Journal of Shandong University (Natural Science) 2023; 58: 121-126. (in Chinese)

[7] Tian, Y., Tu, C., Zhou, Q., et al. The temporal and spatial distribution and surface morphology of atmospheric microplastics around the Bohai Sea. Acta Scientiae Circumstantiae 2020; 40: 1401-1409. (in Chinese)

[8] Liu, Z., Bai, Y., Ma, T., et al. Distribution and possible sources of atmospheric microplastic deposition in a valley basin city (Lanzhou, China). Ecotoxicol. Environ. Saf. 2022; 233: 113353.

[9] Zhang, J.J., Ding, W.C., Zou, G.Y., et al. Urban pipeline rainwater runoff is an important pathway for land-based microplastics transport to inland surface water: A case study in Beijing. Sci. Total. Environ. 2023; 861.

[10] Huang, Y., He, T., Yan, M., et al. Atmospheric transport and deposition of microplastics in a subtropical urban environment. J. Hazard. Mater. 2021; 416: 126168.
[11] Wang, Z., Zhang, Y., Kang, S., et al. Long-range transport of atmospheric microplastics deposited onto glacier in southeast Tibetan Plateau. Environ. Pollut. 2022; 306: 119415.
[12] Ambrosini, R., Azzoni, R.S., Pittino, F., et al. First evidence of microplastic contamination in the supraglacial debris of an alpine glacier. Environ. Pollut. 2019; 253: 297-301.
[13] Dong, H., Wang, L., Wang, X., et al. Microplastics in a Remote Lake Basin of the Tibetan Plateau: Impacts of Atmospheric Transport and Glacial Melting. Environ. Sci. Technol. 2021; 55: 12951-12960.
[14] Tang, L., Feng, J.C., Li, C., et al. Global occurrence, drivers, and environmental risks of microplastics in marine environments. J. Environ. Manage. 2023; 329: 116961.
[15] Marti, E., Martin, C., Galli, M., et al. The Colors of the Ocean Plastics. Environ. Sci. Technol. 2020; 54: 6594-6601.
[16] Huang, L., Li, Q., Xu, X., et al. Composition and distribution of microplastics in the surface seawater of Xisha Islands. Chinese Science Bulletin 2020; 65: 2627-2635. (in Chinese)
[17] Xu, C., Zhang, B., Gu, C., et al. Are we underestimating the sources of microplastic pollution in terrestrial environment? J. Hazard. Mater. 2020; 400: 123228.
[18] Feng, S.S., Lu, H.W., Yao, T.C., et al. Microplastic footprints in the Qinghai-Tibet Plateau and their implications to the Yangtze River Basin. J. Hazard. Mater. 2021; 407.
[19] Xia, W., Rao, Q., Deng, X., et al. Rainfall is a significant environmental factor of microplastic pollution in inland waters. Sci. Total. Environ. 2020; 732: 139065.
[20] Liu, M.T., Lu, S.B., Song, Y., et al. Microplastic and mesoplastic pollution in farmland soils in suburbs of Shanghai, China. Environ. Pollut. 2018; 242: 855-862.
[21] Zhang, H.R., Jin, T., Geng, M.J., et al. Occurrence of Microplastics from Plastic Fragments in Cultivated Soil of Sichuan Province: The Key Controls. Water 2022; 14.
[22] Yang, J., Song, K.F., Tu, C., et al. Distribution and weathering characteristics of microplastics in paddy soils following long-term mulching: A field study in Southwest China. Sci. Total. Environ. 2023; 858.
[23] Wang, J., Li, J.Y., Liu, S.T., et al. Distinct microplastic distributions in soils of different land-use types: A case study of Chinese farmlands. Environ. Pollut. 2021; 269.
[24] Xu, L., Xu, X.B., Li, C., et al. Is mulch film itself the primary source of meso- and microplastics in the mulching cultivated soil? A preliminary field study with econometric methods. Environ. Pollut. 2022; 299.
[25] Yu, L., Zhang, J.D., Liu, Y., et al. Distribution characteristics of microplastics in agricultural soils from the largest vegetable production base in China. Sci. Total. Environ. 2021; 756.
[26] Feng, S.S., Lu, H.W., Liu, Y.L. The occurrence of microplastics in farmland and grassland soils in the Qinghai-Tibet plateau: Different land use and mulching time in facility agriculture. Environ. Pollut. 2021; 279.
[27] Bi, D., Wang, B., Li, Z., et al. Occurrence and distribution of microplastics in coastal plain soils under three land-use types. Sci. Total. Environ. 2023; 855: 159023.
[28] Liu, X.N., Tang, N., Yang, W.G., et al. Microplastics pollution in the soils of various land-use types along Sheshui River basin of Central China. Sci. Total. Environ. 2022; 806.
[29] Chen, L., Yu, L., Li, Y., et al. Spatial Distributions, Compositional Profiles, Potential Sources, and Intfluencing Factors of Microplastics in Soils from Different Agricultural Farmlands in China: A National Perspective. Environ. Sci. Technol. 2022; 56: 16964-16974.

Table S6. Parameters and chemical composition of cloud water at Mt. Tai during summer 2021.

	Unit	Range	Mean		Unit	Range	Mean
Abundance	MP L^{-1}	0-1154	462.6	Ca^{2+}	mg L^{-1}	0.05-11.48	3.03
NC	# m^{-3}	137-11053	3038	Mg^{2+}	mg L^{-1}	0.7-1.28	0.87
LWC	g m^{-3}	0.04-2.65	0.45	F^-	mg L^{-1}	0.03-0.88	0.18
pH		6.12-6.99	6.63	Cl^-	mg L^{-1}	0.02-3.76	1.18
EC	us m^{-3}	22.8-617	121.5	Br^-	mg L^{-1}	0.02-0.82	0.23
DOC	mg L^{-1}	1.66-33.57	8.90	NO_3^-	mg L^{-1}	3.05-101.47	20.73
NH_4^+	mg L^{-1}	1.29-46.34	10.6	SO_4^{2-}	mg L^{-1}	1-58.83	12.99
K^+	mg L^{-1}	0.02-1.17	0.32				

Literature

(1) Ye, C.; Xue, C. Y.; Zhang, C. L.; Ma, Z. B. A.; Liu, P. F.; Zhang, Y. Y.; Liu, C. T.; Zhao, X. X.; Zhang, W. J.; He, X. W.; Song, Y. F.; Liu, J. F.; Wang, W. H.; Sui, B. H.; Cui, R.; Yang, X.; Mei, R. B.; Chen, J. M.; Mu, Y. J., Atmospheric Hydrogen Peroxide (H2O2) at the Foot and Summit of Mt. Tai: Variations, Sources and Sinks, and Implications for Ozone Formation Chemistry. *J. Geophys. Res. Atmos.* **2021,** *126*, (15).

(2) Li, T.; Wang, Y.; Mao, H.; Wang, S.; Talbot, R. W.; Zhou, Y.; Wang, Z.; Nie, X.; Qie, G., Insights on Chemistry of Mercury Species in Clouds over Northern China: Complexation and Adsorption. *Environ. Sci. Technol.* **2018,** *52*, (9), 5125-5134.

(3) Luo, X.; Wang, Z.; Yang, L.; Gao, T.; Zhang, Y., A review of analytical methods and models used in atmospheric microplastic research. *Sci. Total. Environ.* **2022,** *828*, 154487.

(4) Dong, H.; Wang, L.; Wang, X.; Xu, L.; Chen, M.; Gong, P.; Wang, C., Microplastics in a Remote Lake Basin of the Tibetan Plateau: Impacts of Atmospheric Transport and Glacial Melting. *Environ. Sci. Technol.* **2021,** *55*, (19), 12951-12960.

(5) Bergmann, M.; Mützel, S.; Primpke, S.; Tekman, M. B.; Trachsel, J.; Gerdts, G., White and wonderful? Microplastics prevail in snow from the Alps to the Arctic. *Sci. Adv.* **2019,** *5*, (8), eaax1157.

(6) Allen, S.; Allen, D.; Phoenix, V. R.; Le Roux, G.; Durántez Jiménez, P.; Simonneau, A.; Binet, S.; Galop, D., Atmospheric transport and deposition of microplastics in a remote mountain catchment. *Nat. Geosci.* **2019,** *12*, (5), 339-344.

(7) Allen, S.; Allen, D.; Baladima, F.; Phoenix, V. R.; Thomas, J. L.; Le Roux, G.; Sonke, J. E., Evidence of free tropospheric and long-range transport of microplastic at Pic du Midi Observatory. *Nat. Commun.* **2021,** *12*, (1), 7242.

(8) Li, Y.; Zhang, Y.; Su, F.; Wang, Y.; Peng, L.; Liu, D., Adsorption behaviour of microplastics on the heavy metal Cr(VI) before and after ageing. *Chemosphere* **2022,** *302*, 134865.

(9) Mao, R.; Lang, M.; Yu, X.; Wu, R.; Yang, X.; Guo, X., Aging mechanism of microplastics with UV irradiation and its effects on the adsorption of heavy metals. *J. Hazard. Mater.* **2020,** *393*, 122515.

(10) Liu, P.; Zhan, X.; Wu, X.; Li, J.; Wang, H.; Gao, S., Effect of weathering on environmental behavior of microplastics: Properties, sorption and potential risks. *Chemosphere* **2020,** *242*, 125193.

(11) Xu, X.; Zhen, J.; Jiang, Y.; Du, P.; yuan, X.; Wu, D.; Yin, X.; Wang, Y., Characteristics and

sources analysis of microplastics in precipitation of Mount Tai. *Journal of Shandong University (Natural Science)* **2023,** *58*, (3), 121-126.
(12) Allen, S.; Allen, D.; Moss, K.; Le Roux, G.; Phoenix, V. R.; Sonke, J. E., Examination of the ocean as a source for atmospheric microplastics. *PLoS One* **2020,** *15*, (5), e0232746.
(13) Wang, Y.; Okochi, H.; Tani, Y.; Hayami, H.; Minami, Y.; Katsumi, N.; Takeuchi, M.; Sorimachi, A.; Fujii, Y.; Kajino, M.; Adachi, K.; Ishihara, Y.; Iwamoto, Y.; Niida, Y., Airborne hydrophilic microplastics in cloud water at high altitudes and their role in cloud formation. *Environ. Chem. Lett.* **2023,** *21*, 3055–3062.
(14) Abbasi, S.; Turner, A., Dry and wet deposition of microplastics in a semi-arid region (Shiraz, Iran). *Sci. Total. Environ.* **2021,** *786*, 147358.
(15) Wang, Z.; Zhang, Y.; Kang, S.; Yang, L.; Luo, X.; Chen, P.; Guo, J.; Hu, Z.; Yang, C.; Yang, Z.; Gao, T., Long-range transport of atmospheric microplastics deposited onto glacier in southeast Tibetan Plateau. *Environ. Pollut.* **2022,** *306*, 119415.
(16) Aves, A. R.; Revell, L. E.; Gaw, S.; Ruffell, H.; Schuddeboom, A.; Wotherspoon, N. E.; LaRue, M.; McDonald, A. J., First evidence of microplastics in Antarctic snow. *Cryosphere* **2022,** *16*, (6), 2127-2145.
(17) Liu, K.; Wang, X.; Fang, T.; Xu, P.; Zhu, L.; Li, D., Source and potential risk assessment of suspended atmospheric microplastics in Shanghai. *Sci. Total. Environ.* **2019,** *675*, 462-471.
(18) Dris, R.; Gasperi, J.; Mirande, C.; Mandin, C.; Guerrouache, M.; Langlois, V.; Tassin, B., A first overview of textile fibers, including microplastics, in indoor and outdoor environments. *Environ. Pollut.* **2017,** *221*, 453-458.
(19) Ding, Y.; Zou, X.; Wang, C.; Feng, Z.; Wang, Y.; Fan, Q.; Chen, H., The abundance and characteristics of atmospheric microplastic deposition in the northwestern South China Sea in the fall. *Atmos. Environ.* **2021,** *253*, 118389.
(20) Liu, K.; Wu, T.; Wang, X.; Song, Z.; Zong, C.; Wei, N.; Li, D., Consistent Transport of Terrestrial Microplastics to the Ocean through Atmosphere. *Environ. Sci. Technol.* **2019,** *53*, (18), 10612-10619.
(21) Wang, X.; Li, C.; Liu, K.; Zhu, L.; Song, Z.; Li, D., Atmospheric microplastic over the South China Sea and East Indian Ocean: abundance, distribution and source. *J. Hazard. Mater.* **2020,** *389*, 121846.